

# **Weakening of Jammed Subduction Shear Zones, Leading to the Generation of Slow Slip Events**

Adam Beall<sup>1</sup>, Ake Fagereng<sup>1</sup> and Susan Ellis<sup>2</sup>

<sup>1</sup>*School of Earth and Ocean Sciences, Cardiff University, UK*

<sup>2</sup>*GNS Science, Avalon, Lower Hutt, NZ*

---

*This manuscript is a non-peer-reviewed preprint  
submitted to Geochemistry, Geophysics, Geosystems*

---

1 **Fracture and Weakening of Jammed Subduction Shear**  
2 **Zones,**  
3 **Leading to the Generation of Slow Slip Events**

4 **Adam Beall<sup>1</sup>, Åke Fagereng<sup>1</sup> and Susan Ellis<sup>2</sup>**

5 <sup>1</sup>School of Earth and Ocean Sciences, Cardiff University, Cardiff, UK

6 <sup>2</sup>GNS Science, Avalon, Lower Hutt, New Zealand

7 **Key Points:**

- 8 • Fracturing of clasts in a mélange with viscosity contrasts of  $10^3$  occurs at applied  
9 stresses 80% lower than for a homogeneous fault
- 10 • Fracturing of clasts in load-bearing force chains leads to stress redistribution into  
11 the viscously creeping matrix
- 12 • A transient reduction in clast strength by 75% can increase mélange strain-rate  
13 by  $8\times$ , potentially generating a slow slip event

---

Corresponding author: Adam Beall, [bealla1@cardiff.ac.uk](mailto:bealla1@cardiff.ac.uk)

**Abstract**

Geodetic data have revealed that parts of subduction interfaces creep steadily or transiently. Transient slow slip events (SSEs) are typically interpreted as aseismic frictional sliding. However, SSEs may also occur via mixed visco-brittle deformation, as observed in exhumed shear zones containing mixtures (mélange) of strong fractured clasts embedded in a weak visco-brittle matrix. We test the hypothesis that creep in a subduction mélange occurs through distributed matrix deformation, where flow is modified and impeded by load-bearing clast networks. Our numerical models demonstrate that bulk mélange rheology can be dominated by the strong clasts in the absence of fracturing, while at high driving stresses or low frictional strength, clast fracturing redistributes deformation into the matrix, leading to high bulk strain-rates. Mélange stress is highly heterogeneous, fracturing some clasts even when the bulk mélange stresses are only 20% of the clast yield strength, though with minor strain-rate increase due to clast stress redistribution. Transient strain-rate increases have previously been modelled as periods of lowered frictional strength. Mélange clasts must weaken significantly ( $\sim 75\%$ ) in order to increase strain-rate by 8x. Frictional weakening could occur through the formation of extension or extensional-shear fractures in clasts, as observed within shear networks in exhumed mélange outcrops. We outline a model where high bulk strain-rates are generated when pervasive fracturing occurs, but further slip is limited by viscous processes. Incorporating such viscous damping into models may widen the conditions under which SSEs can occur while preventing development of seismic slip.

**Plain Language Summary**

While some subduction zones are responsible for generating large, devastating earthquakes, others creep steadily or episodically. This range of deformation styles may correspond to the varying interaction of viscous creep and frictional failure, as observed in exhumed subduction shear zones, which are typically mixtures (mélanges) of strong fractured and weak viscous materials. We use computer models to explore how mélange strength and deformation style varies when the frictional material fractures. Load-bearing networks of unfractured strong material contribute significantly to mélange strength, so the onset of fracturing redistributes some deformation into the weak viscous material. As the force distribution in these networks is complicated, the onset of frictional failure alone is insufficient to completely unload the strong material. However, if the frictional ma-

46 terial weakens considerably, as may occur when fractures open, *mélange* may undergo  
47 a period of rapid, predominately viscous deformation. Cycles of viscous deformation may  
48 correspond to episodic creep events. If creep events do occur primarily by a viscous mech-  
49 anism, this may explain why they can occur routinely in some regions without transi-  
50 tioning to seismic slip.

## 51 **1 Introduction**

52 The rheology and frictional properties of the subduction thrust interface exert a  
53 first-order control on the generation of major earthquakes (Scholz, 1998) and the max-  
54 imum sustainable stresses and deformation rates at a convergent margin (Duarte et al.,  
55 2015; Behr & Becker, 2018). The down-dip limit of a subduction thrust seismogenic zone  
56 is often thought to be limited by the onset of steady viscous creep at temperatures  $>350^{\circ}$   
57 (e.g. Hyndman et al., 1997). Slow slip events (SSEs), episodes of aseismic slip  $\sim 0.1 - 1$   
58 m/year (faster than plate velocities) and commonly associated with tectonic tremor, have  
59 been observed in this transition zone (Rogers & Dragert, 2003; Schwartz & Rokosky, 2007).  
60 These events require an evolution in our understanding of the gradual spatial transition  
61 between the seismogenic zone and deeper, steady aseismic creep. SSEs have been pri-  
62 marily considered to arise due to frictional dynamics (Liu & Rice, 2005; Leeman et al.,  
63 2018). It has also been proposed that SSEs are the result of dynamic interaction between  
64 viscous and frictional deformation (Ando et al., 2012; Fagereng et al., 2014; Hayman &  
65 Lavier, 2014), though it is still unclear which visco-brittle rheological model is most ap-  
66 propriate.

67 *Mélange*, a mixture of strong clasts embedded in a weak matrix, is commonly found  
68 in exhumed subduction-related shear zones and in some places preserves a mixture of  
69 contemporaneously formed brittle and ductile structures resulting from the interplay be-  
70 tween strong (brittle) clasts and weak (ductile) matrix (Fagereng & Sibson, 2010). Ma-  
71 trix deformation is typically distributed, likely as a result of a predominately creeping  
72 process such as pressure solution, as observed at the  $\mu\text{m}$  scale in fine-grained phyllosil-  
73 icates, quartz and calcite, in combination with dilation of frictionally weak phyllosilicate  
74 cleavage (Bos & Spiers, 2001; Kitamura et al., 2005; Rowe et al., 2011; Wassmann & Stöckhert,  
75 2013; Fagereng & den Hartog, 2016). Such pressure solution may be responsible for sub-  
76 duction interface creep. Fractures within the *mélange*, predominately found in clasts, are  
77 indicative of locally high strength and stress (in the absence of extreme pore pressure

78 variation). Depending on the connectivity of these high stress clasts, there may be no  
79 connected matrix pathways for simple shear to occur, in which case the *mélange* rheol-  
80 ogy will be strong (referred to as jammed) and dependent on clast fracturing. Such load-  
81 bearing networks are called force chains and their reorganisation is responsible for stick-  
82 slip events in granular materials (Hayman et al., 2011). As a result of force chain dy-  
83 namics, the observed viscous and brittle *mélange* deformation may preserve cycles of al-  
84 ternating deformation mechanisms, perhaps generating SSEs.

85 Viscous creep, for example pressure solution of quartz, can stabilise sliding along  
86 adjacent frictional minerals (Niemeijer, 2018), producing velocity-strengthening behaviour.  
87 Velocity-strengthening parts of a subduction interface can produce an SSE by dampen-  
88 ing an otherwise unstable rupture initiating in velocity-weakening material (Skarbek et  
89 al., 2012; Luo & Ampuero, 2018). Analogue models show that slow stick-slip events can  
90 occur in a macroscopically homogeneous viscoplastic material likely due to reorganisa-  
91 tion of microgel force chains (Reber et al., 2015; Birren & Reber, 2019). Microscopically,  
92 these events are related to reorganisation of force chains, while macroscopically they cor-  
93 respond to episodic opening of tensile fractures, which grade into shear fractures and vis-  
94 cious deformation accommodating overall simple shear. In contrast, slow stick-slip events  
95 have been produced in rock experiments at normal stresses of  $< 10$  MPa and high ( $>0.9$ )  
96 apparatus to critical stiffness ratios (Kaproth & Marone, 2013; Scuderi et al., 2017; Lee-  
97 man et al., 2018). Visco-brittle interactions are difficult to quantify in such experiments,  
98 but microstructural observations indicate that frictional instabilities occur when defor-  
99 mation localizes in shear bands, and slip style may be controlled by the interplay between  
100 the rheology of such shear bands and the surrounding fault rock (Scuderi et al., 2017).  
101 It is, however, still unclear if ductile and brittle interactions are necessary to produce  
102 strain-rate transients such as SSEs, and if rheological interactions do occur, what are the  
103 fundamental processes and scales at which they operate.

104 *Mélange* rheology can be dominated by weak matrix constituents if there are con-  
105 nected matrix shear pathways that accommodate bulk simple shear (Handy, 1994). How-  
106 ever, finite element models (Webber et al., 2018; Beall et al., 2019) demonstrate that mi-  
107 nor shear strain of *mélange* with around 50% or more ellipsoidal clasts leads to the for-  
108 mation of clast force chains which block matrix pathways (Fig. 1a), switch the *mélange*  
109 to clast-dominated deformation (jamming), and consequently decrease strain-rate by more  
110 than an order of magnitude. We explore the hypothesis that such force chains may be

111 disabled through the fracturing of clasts as their yield strength is reached after jamming  
 112 (Fig. 1b), which redistributes stress into the matrix. This increase in matrix stress would  
 113 consequently increase the bulk shear zone strain-rate. If this hypothesis is correct, mélange  
 114 deformation would temporarily switch between being limited by frictional failure and be-  
 115 ing controlled by viscous creep, as proposed in previous models (Lavier et al., 2013; Re-  
 116 ber et al., 2015). Geological evidence for such visco-brittle interaction indicates this pro-  
 117 cess could occur from centimetre up to 100s of metre scales (Fagereng & Sibson, 2010;  
 118 Fagereng, 2011a; Rowe et al., 2011; Grigull et al., 2012; Hayman & Lavier, 2014). To in-  
 119 tegrate shear zone dynamics into large scale models, mélange deformation must be pa-  
 120 rameterized into a bulk rheology relating effective stresses to strain-rates and/or strain  
 121 (see Section 2, below).

122 Mélangé clasts are commonly fractured, despite the low differential stress implied  
 123 by creep of adjacent matrix. While fracturing is typically thought to indicate near-lithostatic  
 124 pore-pressure (e.g. Sibson, 1996), Beall et al. (2019) showed that clast shear stress can  
 125 be increased by  $> 3\times$  due to the viscosity contrast between clasts and matrix, even in  
 126 the absence of a force chain network. These models did not incorporate fracturing, so  
 127 it is unclear how pervasive fracturing would be and how it affects mélange rheology. Mélangé  
 128 fracture kinematics are typically consistent with matrix simple shear (Fagereng, 2011b).  
 129 Fractures are also commonly confined to clasts or transition into terminating shear frac-  
 130 tures in the matrix (Fisher & Byrne, 1987; Raimbourg et al., 2009; Fagereng, 2013). While  
 131 these observations support a model of contemporaneous frictional and viscous deforma-  
 132 tion, it is unclear how frictional failure would affect the bulk mélange rheology. In this  
 133 study, we incorporate fracturing into our numerical mélange models and quantify both  
 134 1) how pervasive clast fracturing is at varying shear zone stress, and 2) whether fractur-  
 135 ing could effectively disable force chains and increase shear zone strain-rates.

## 136 **2 Bulk Rheology of a Subduction Interface: Theoretical Mixture Model** 137 **Predictions**

138 Geodynamic models of visco-brittle subduction interface deformation typically com-  
 139 bine one viscous and one brittle rheology into a composite rheology (Karato, 2012), fol-  
 140 lowing the assumption that both rheologies experience either the same stress (the Reuss  
 141 model) or the same strain (the Voigt model). The choice of Reuss or Voigt model dic-  
 142 tates which rheology dominates at low and high stress (Fig. 1c).

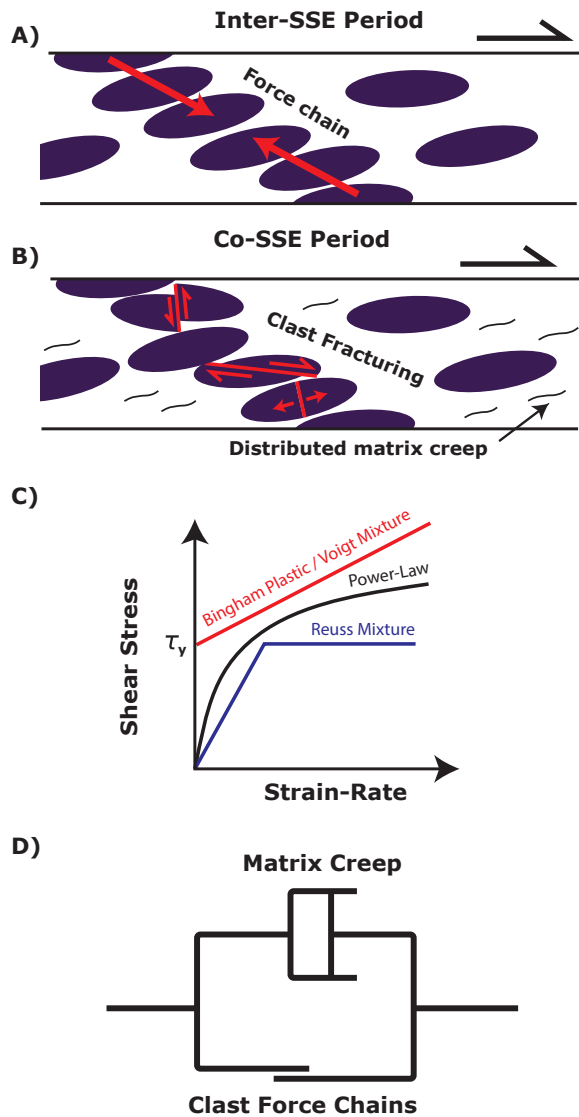


**Figure 1.** A) Periods of low megathrust creep in-between SSEs are hypothesised to be due to the formation of clast force chains, which prevent viscous matrix deformation. B) When clasts fracture, stress may be redistributed to the weak matrix, switching the mélange to predominately viscous deformation with a high strain-rate. C) Schematic comparison of the Voigt (equivalent to Bingham plastic) and Reuss mixture models (and comparison to power-law rheology). When fracturing begins at  $\tau = \tau_y$  (or lower if stress amplification is considered), the Voigt model is rate-limited by viscous deformation, while the Reuss model becomes stress-limited by frictional deformation (which may be modestly rate-strengthening or weakening, or constant as shown here). D) We hypothesise that the rheology of a jammed mélange can be modelled as a viscous dashpot (matrix creep) in parallel with a frictional slider (fracture of clasts, neglecting their slow viscous creep), equivalent to a Bingham plastic.

143 The Reuss model represents material that can always viscously flow (though slowly  
 144 for high viscosities), but switch to frictional deformation if a yield stress is reached. For  
 145 predominately viscous slip transients to occur in a Reuss mixture, the viscous rheology  
 146 must be highly non-linear (e.g. incorporating shear heating; Goswami & Barbot, 2018).  
 147 The Voigt model, which is equivalent to a Bingham plastic when one of the materials  
 148 is frictional (Fig. 1c), represents a material that does not deform at all until frictional  
 149 sliding occurs, at which point viscous deformation becomes rate-limiting and a low vis-  
 150 cosity may produce high strain-rates (used by Ando et al., 2012; Lavier et al., 2013).  
 151 Stress-dependent viscous deformation is generally captured by the power-law rheology  
 152  $\dot{\epsilon} \propto \sigma^n$  (Fig. 1c) for maximum shear strain-rate  $\dot{\epsilon}$  and stress  $\tau$  (Karato, 2012). The mag-  
 153 nitude of the stress exponent  $n$  dictates how stress-dependent the rheology is, for exam-  
 154 ple  $n \approx 3$  for dislocation creep and  $n \rightarrow \infty$  for a plastic material with a yield strength.  
 155 It is unclear which model best captures the rheology of a subduction interface shear zone.

156 If a *mélange* only deforms when clasts in a force chain can deform, then assuming  
 157 that clast and matrix strain is equal will give the Voigt / Bingham model. This model  
 158 is supported by GPS records, which generally show that inter-SSE locking is high on in-  
 159 terface patches hosting SSEs (e.g. Wallace & Beavan, 2010). If clast and matrix stresses  
 160 are each homogeneously defined by constants  $\tau_{clast}$  and  $\tau_{matrix}$ , their stresses are related  
 161 to the bulk stress by  $\tau = \phi\tau_{clast} + (1 - \phi)\tau_{matrix}$ . If clasts are purely frictional,  $\tau_{clast}$   
 162 is limited to a yield stress  $\tau_y$ , and if  $\tau_{matrix}$  is controlled by Newtonian viscous creep  $2\eta\dot{\epsilon}$   
 163 (e.g. pressure solution creep), then an effective rheology is given by Eq. 1, i.e. a Bing-  
 164 ham rheology (Fig. 1c-d), where viscous creep occurs if bulk *mélange* stress  $\tau \geq \phi\tau_y$ .

$$\tau = \phi\tau_y + 2(1 - \phi)\eta\dot{\epsilon} \quad (1)$$

165 This simple model predicts that frictional failure and the activation of viscous flow  
 166 occurs at a bulk stress which is lower than the frictional clast strength, as stress is fo-  
 167 cussed into only the clast volume (controlled by  $\phi$ ). This stress amplification has been  
 168 shown to occur in models with complex force chain geometries, where frictional yield oc-  
 169 curs for bulk stresses well below the clast yield limit due to the clast-matrix viscosity con-  
 170 trast (Beall et al., 2019). Eq. 1 also predicts that the viscous strain-rate will be zero when  
 171 frictional failure first occurs, as  $\tau_{matrix} = 0$  when  $\tau = \phi\tau_y$ , unless  $\tau_y$  is dynamically  
 172 decreased or  $\tau$  is increased further. Clast stresses are not, however, likely to be homo-



173 geneous for realistic force chain geometries and matrix strain-rate will not be completely  
 174 zero, so the predicted stress for the onset of visco-brittle deformation is an approximate  
 175 guide.

### 176 **3 Methodology**

177 The modelling methodology is adapted from Beall et al. (2019), in which a New-  
 178 tonian viscous *mélange* was modelled as lens-shaped clasts embedded in a matrix, where  
 179 the clasts had a viscosity  $10\text{--}10^4\times$  higher than the matrix. The velocity at the top bound-  
 180 ary was derived by applying a constant driving stress, allowing an effective strain-rate  
 181 and bulk viscosity to be calculated, as well as the *mélange* stress distribution, as a func-  
 182 tion of the viscosity contrast, clast proportion  $\phi$  and shear zone thickness. Jamming of  
 183 *mélange* with a viscosity contrast of  $10^3$  resulted in an effective viscosity increase of 2–  
 184  $7\times$  and clast shear stress of  $6\text{--}9\tau$  (for applied driving stress  $\tau$ ), over the range  $0.5 \leq$   
 185  $\phi \leq 0.64$ . Here, we build upon these previous models by incorporating frictional fail-  
 186 ure into the clast rheology. This study also follows Webber et al. (2018), though is more  
 187 simplified in order to characterise *mélange* rheology in a generalised manner.

188 Shear zone deformation is modelled as incompressible creeping viscous flow, via the  
 189 continuum-mechanics finite-element particle-in-cell code Underworld, which solves the  
 190 Stokes equations. The matrix has a Newtonian viscosity  $\eta_m$ , representing diffusion creep  
 191 processes such as the pressure solution observed in quartz-phyllsilicate mixtures (Bos  
 192 & Spiers, 2001; Fagereng & den Hartog, 2016; Niemeijer, 2018) at temperatures of  $\geq 100^\circ\text{C}$   
 193 and within a range of fine-grained metamorphic assemblages at lower crustal conditions  
 194 (Wassmann & Stöckhert, 2013). Frictional failure is incorporated by checking if each point  
 195 within the clast material has a maximum shear stress  $\tau_{max} = (\sigma_1 - \sigma_2)/2$  (where  $\sigma_1$   
 196 and  $\sigma_2$  are the in-plane principal stresses) exceeding a frictional strength  $\tau_y$ , in which  
 197 case an effective viscosity is iteratively calculated at that point in order to satisfy  $\eta_f =$   
 198  $\frac{1}{2}\tau_y/\dot{\epsilon}_{max}$  (for maximum shear strain-rate  $\dot{\epsilon}_{max}$  at that point in space and time; follow-  
 199 ing Fullsack, 1995; Moresi & Solomatov, 1998). The yield stress is either set to a con-  
 200 stant or to the Coulomb failure criteria Eq. 2, for friction coefficient  $\mu$ , cohesion  $C$  and  
 201 effective mean stress  $\sigma_{eff}$  (Jaeger et al., 2007).

$$\tau_y = \frac{\mu\sigma_{eff} + C}{\sqrt{1 + \mu^2}} \quad (2)$$

**Table 1.** Summary of model-sets and parameters.

Model-set	Frictional Parameters	Clast Proportion ( $\phi$ ) and Maximum Width ( $D_{max}$ )
A	$\mu = 0.7, C = 50\text{MPa}$ ( $\tau_y \approx 160\text{MPa}$ )	$\phi = 0.3, 0.5, 0.61$ ( $D_{max} = 0.14$ ), $\phi = 0.61$ ( $D_{max} = 0.28$ )
B	$\tau_y = 200\text{MPa}$	$\phi = 0.61$ ( $D_{max} = 0.14$ )
C	$\tau_y = 50\text{MPa}$	$\phi = 0.61$ ( $D_{max} = 0.14$ )

202  $\sigma_{eff}$  is calculated as  $(p + \rho gz)(1 - \lambda)$ , where  $p$  is a dynamic pressure deviation from  
 203 the lithostatic pressure,  $\rho$  is the average overburden density set to  $2650 \text{ kg m}^{-3}$ ,  $g$  is grav-  
 204 itational acceleration,  $z$  is depth and  $\lambda$  is the prescribed ratio of pore-pressure to litho-  
 205 static pressure. We study deformation at a depth of  $z = 40 \text{ km}$ , roughly matching the  
 206 depth of SSEs in Cascadia (Rogers & Dragert, 2003), southern Hikurangi (Wallace &  
 207 Beavan, 2010) and the deep SSEs in Nankai (Obara et al., 2004). We assume  $\lambda = 0.8$ ,  
 208 which is intermediate between hydrostatic and lithostatic (Saffer & Tobin, 2011). This  
 209 gives  $\sigma_{eff} \approx 208 \text{ MPa}$  (when  $p = 0$ ) for the models .

210 The model dimensions can be rescaled, in order to explore a wider parameter space.  
 211 We assume that the model stress can be non-dimensionalised as Eq. 3. The accuracy of  
 212 this scaling should vary depending on the degree to which the bulk strain-rate of the melange  
 213 is a function of  $\tau_y$ . We test the applicability of this scaling for jammed melange. It then  
 214 follows that time  $t$  (and therefore strain-rate) can be non-dimensionalised as Eq. 4.

$$\tau' = \frac{\tau}{\tau_y} \quad (3)$$

$$t' = t \frac{\tau_y}{\eta_m} \quad (4)$$

215 We set  $\mu = 0.7$  and  $C = 50 \text{ MPa}$ , representing frictionally strong clasts (e.g. un-  
 216 fractured sandstone or basalt) close to Byerlee’s law (Jaeger et al., 2007). Clast regions  
 217 which do not meet the failure criterion have a Newtonian viscosity set to  $\eta_c = 10^3 \eta_m$ ,  
 218 representing a large viscosity contrast in the melange. We also run models with either  
 219 a high or low constant  $\tau_y$  in order to explore frictional weakening and test our scaling  
 220 predictions (parameters summarised in Table 1).

221 As incompressibility is assumed, deformation involving tensile fracture cannot be  
 222 calculated, but the onset of tensile failure can be predicted. The calculations with vary-  
 223 ing  $\tau_y$  and the scaling approach allow us to explore how mélangé rheology depends on  
 224 clast yield stress, where clast yield includes tensile fracture if it occurs. Tensile failure  
 225 is assumed to occur when minimum in-plane principal stress  $\sigma_2 = T$  for a constant ten-  
 226 sile strength  $T$ . This tensile yield criterion can be rewritten as Eq. 5.

$$\tau_y = \sigma_{eff} + T \quad (5)$$

227 At a specific depth, the Coulomb and tensile failure criteria can be approximated  
 228 by a constant  $\tau_y$  by assuming that the normal stress is equal to the effective lithostatic  
 229 pressure (setting  $p = 0$ ). This neglects normal stress variations within the mélangé, which  
 230 are likely to be small compared to the lithostatic pressure for the 40 km depth modelled.

231 A constant shear traction  $\tau$  is applied to the top model wall, representing the bulk  
 232 shear stress to drive deformation (e.g. Webber et al., 2018). A highly viscous Newtonian  
 233 material with viscosity  $10^3\eta_m$  is included in the upper 5% of the model domain, in or-  
 234 der to distribute this stress within the underlying mélangé. As the bulk rheology of the  
 235 mélangé is of primary interest, a bulk shear strain-rate  $\dot{\epsilon}$  is calculated as  $0.5V_{av}/L$  for  
 236 average horizontal velocity on the top wall  $V_{av}$  and model height  $L$ . We set  $L = 100\text{m}$ ,  
 237 a typical active subduction shear-zone thickness (Rowe et al., 2013) and the model width  
 238 to  $4L$  with periodic boundary conditions. The velocity magnitude is set to zero on the  
 239 lower boundary. The element resolution is  $2048 \times 512$ , equivalent to a mesh node spac-  
 240 ing of 4.9 cm for  $L = 100\text{m}$ .

241 The ratio of the clast short-axis length to the shear zone width ( $L = 100\text{m}$ ) is de-  
 242 fined as  $D$ . Within most models,  $D$  varies from over  $0.05 \leq D \leq 0.14$  (labelled as  $D_{max} =$   
 243  $0.14$ , Table 1). This choice of  $D_{max}$  results in a force chain length scale which is smaller  
 244 than  $L$  and therefore a conservative estimate of jamming (Beall et al., 2019). A model  
 245 with clasts of size  $0.1 \leq D \leq 0.28$  is also included ( $D_{max} \leq 0.28$ ) for  $\phi = 0.64$ , with  
 246 identical model resolution and dimensions, in order to test whether the choice of  $D_{max}$   
 247 affects the bulk visco-brittle rheology. All clasts have a short to long axis ratio of 3. Their  
 248 sizes are chosen to follow a power-law distribution with exponent -2, reflecting clast size  
 249 distributions in visco-brittle shear zones (Fagereng, 2011a; Grigull et al., 2012). As the  
 250 clast geometries are fractal (though limited to a minimum clast size due to the limited

251 mesh resolution), the clast sizes can be scaled up to thicker shear zones with larger clasts  
 252 or down to cm-m scale shear zones. Calculations of stress-strain-rate relationships are  
 253 therefore scale-invariant, provided our clast geometries and simplified rheologies hold.  
 254 Such scaling is limited at the large scale by the largest clast dimension (blocks up to 100  
 255 m long have been observed; Grigg et al., 2012) and the breakdown of the simplified rhe-  
 256 ology at the small scale (grain-scale processes are critical at and below the mm scale; Fagereng  
 257 & den Hartog, 2016).

258 As the clasts are originally randomly orientated and with minimal force chains present,  
 259 a setup model is run for each volumetric clast proportion  $\phi$  up to a shear strain of  $\epsilon =$   
 260 2 to generate a strained *mélange* with force chains (if  $\phi$  is sufficiently high). This is used  
 261 as a starting material distribution for the main model experiments. The setup runs ne-  
 262 glect clast fracturing, for both computational efficiency (numerical iterations are not re-  
 263 quired) and to provide identical starting conditions for all models with a given  $\phi$ . The  
 264 setup strain is sufficient for force chains to form (where  $\phi$  is high enough), though fur-  
 265 ther jamming may occur at higher strain. *Mélange* formation through disaggregation of  
 266 stratigraphy and significant simple shear has been inferred to occur before and during  
 267 lithification (Fagereng, 2011b; Festa et al., 2012). Our initial conditions could therefore  
 268 apply to any depth.

## 269 4 Results

### 270 4.1 Simplified Force Chain Model

271 We firstly test the applicability of Eq. 1, an idealised Voigt (iso-strain) mixture /  
 272 Bingham rheology, to an idealised numerical model. The visco-brittle clast rheology is  
 273 assigned to one column orientated at  $45^\circ$  to the horizontal in the direction of greatest  
 274 compressive stress. This column represents a force chain, is assigned a constant  $\tau_y =$   
 275 170 MPa, a width giving  $\phi = 0.1$  and is embedded in a viscous matrix (Fig. 2a). Eq.  
 276 1 predicts onset of creeping for a bulk stress of 17 MPa. In the numerical model, the in-  
 277 stantaneous strain-rate was calculated for a variety of boundary shear stress magnitudes.  
 278 The simple force chain model almost exactly matches Eq. 1, with the minor exception  
 279 of a non-zero, though negligible, strain-rate when  $\tau < \phi\tau_y$  due to the model clast rhe-  
 280 ology being viscoplastic rather than perfectly plastic (i.e. in the numerical model creep  
 281 is allowed when  $\tau_{max} < \tau_y$ ). The Bingham rheology therefore has the potential to cap-

282 ture the bulk rheology of a numerical model when the iso-strain (Voigt) assumption holds.  
 283 Whether this holds for complicated force chain geometries is explored in the following  
 284 sections.

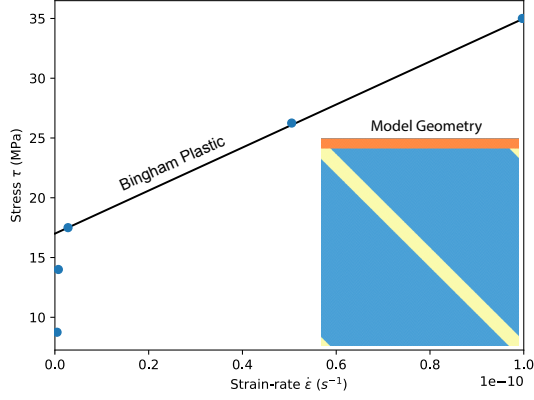
## 285 4.2 Melange Fracturing at Low Melange Boundary Stress

286 We use Model-set A (Table 1) as a strong end-member to test whether stress-amplification  
 287 leads to significant fracturing even at bulk stresses much lower than the clast yield stress.  
 288 For a depth of 40 km, fluid-pressure ratio  $\lambda = 0.8$  and in the case that  $p = 0$ , the fric-  
 289 tional parameters for set A give a yield stress  $\tau_y = 160$  MPa (Eq. 2). Results show that  
 290 all models, including for applied stress as low as  $\tau = 21$  MPa (non-dimensionalised  $\tau' =$   
 291  $0.13$ ), involved some clast yielding, in which case the clast  $\eta_{eff}$  locally reduces by at least  
 292 an order of magnitude (in order to satisfy  $\tau_{max} = \tau_y$ ). As we are interested in how frac-  
 293 turing affects dynamics at the shear-zone scale, a better measure of the lower threshold  
 294 for fracturing is the lowest bulk stress  $\tau$  modelled for which there is a chain of fractur-  
 295 ing clasts spanning  $L$ . In this case, fracturing occurs at  $\tau \geq 35$  MPa ( $\tau' \geq 0.22$ , Fig.  
 296 3) for  $\phi = 0.5$ ,  $D_{max} = 0.28$  and  $\phi = 0.61$ ,  $D_{max} = 0.14$ , while fracturing requires  
 297  $\tau \geq 70$  MPa ( $\tau' \geq 0.44$ ) for  $\phi = 0.5$  and  $\phi = 0.3$ ,  $D_{max} = 0.14$ . This shows that sig-  
 298 nificant fracturing can occur when applied stress  $\tau$  is substantially less than  $\tau_y$ , partic-  
 299 ularly for jammed melange and a volumetric clast proportion  $> 50\%$ , owing to stress  
 300 amplification in the clasts.

301 Clast fracturing occurs at low ratios of driving stress to clast yield stress,  $\tau' = 0.22$ .  
 302 The occurrence of fracturing only depends on  $\tau'$  (as demonstrated in Section 4.4) and  
 303 can therefore be used to calculate the driving stress  $\tau$  required to generate fracturing for  
 304 a specified  $\tau_y$ , including for tensile failure. Assuming  $T = 3.5$  MPa (the ratio of C to  
 305 T is typically  $\approx 15$  for sandstone and greater for crystalline rocks; Jaeger et al., 2007),  
 306 then the corresponding yield stress for tensile failure is  $\tau_y = 211$  MPa (Eq. 5). A driv-  
 307 ing stress of  $\tau = 42$  MPa (equivalent to  $\tau' = 0.22$ ), could then generate tensile frac-  
 308 turing. Driving shear stresses of  $\sim 10$  MPa are therefore sufficient to generate shear and/or  
 309 tensile fracturing of clasts at  $z = 40$ km when  $\lambda = 0.8$  (the dominant fracture mode  
 310 depending on the orientation of existing weak planes).

311 The Coulomb failure criterion may be satisfied by shear in two conjugate directions.  
 312 However, simple shear is expected to be accommodated by sliding predominately along

A)



B)

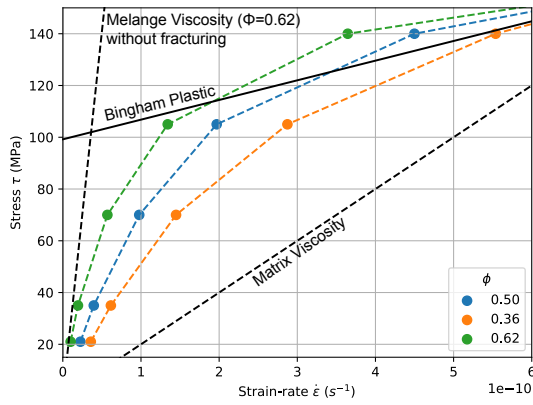


**Figure 2.** Comparisons of idealised (A) and *mélange* (B) force chain models to the Bingham plastic rheology. A) Model geometry, inset, of clast material (yellow,  $\phi = 0.1$ ) embedded in matrix (blue) with high viscosity 'grip' material on top (orange). Measurements of  $\tau$  (points) follow the Bingham plastic rheology (solid line, Eq. 1). B) Model-set A data (for  $D_{max} = 14\text{m}$ ), compared to the Bingham rheology and *mélange* viscosity in the absence of fracturing, for  $\phi = 0.62$ , as well as  $\eta_m$ .

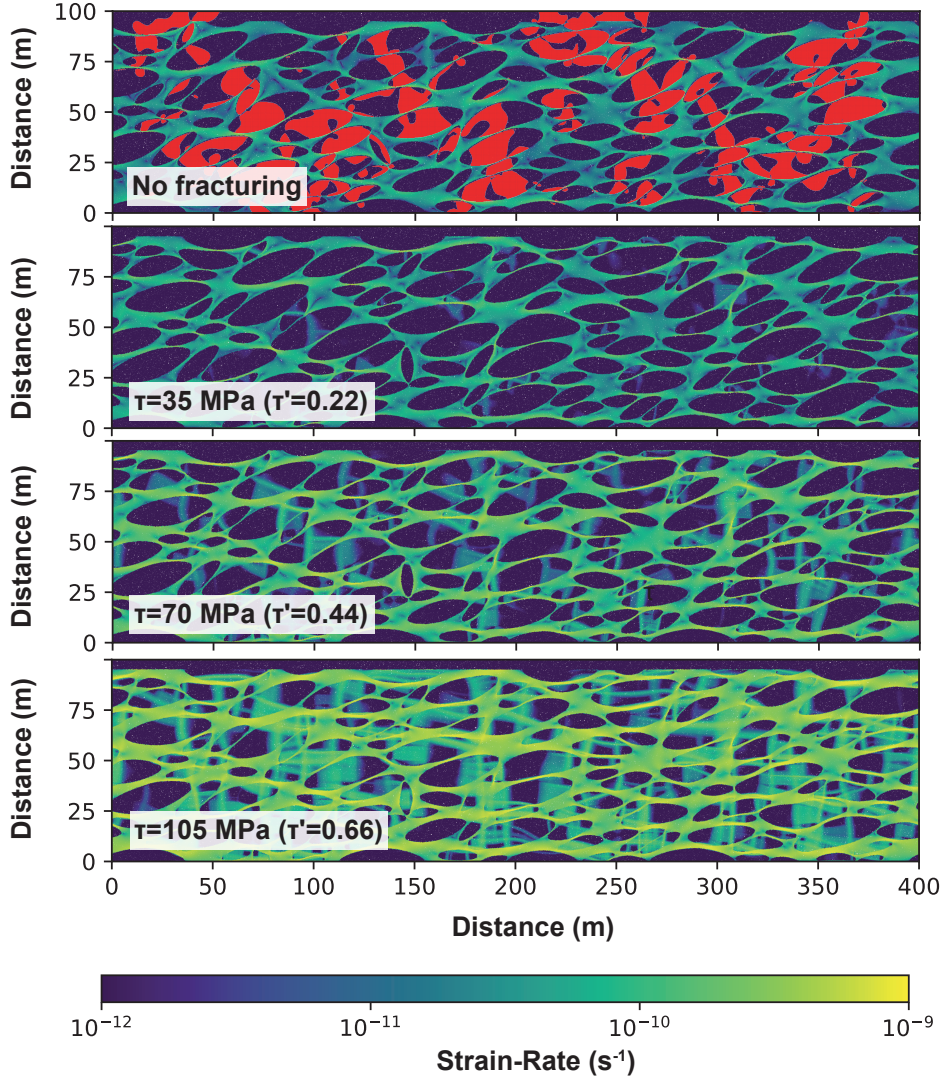


**Figure 3.** Mélange from model-set A with  $\phi = 0.62$ ,  $D_{max} = 14\text{m}$  and  $\eta_m = 10^{17}$  Pa s. For reference, a model with  $\tau = 35$  MPa, fracturing prevented and regions with maximum shear stress increased above  $\tau$  by  $\geq 5\times$  colored red. Models with  $\tau$  varying from 35 to 105 MPa are also shown, demonstrating that the number of clasts reaching the frictional failure criterion increases dramatically with increasing  $\tau$  and contributes to a significantly higher matrix strain-rate at high  $\tau'$  compared to a linear rheology.

313 planes sub-parallel to the shear zone boundary in order to satisfy mass conservation in  
 314 a homogeneous shear zone with constant thickness. Shear along planes sub-parallel to  
 315 the shear zone boundary is also the most efficient way of localising simple shear defor-  
 316 mation, as no rotation or fracture network is required. Yielding in the models, however,  
 317 is localised into conjugate sets of failure planes (Fig. 3). Conjugate sets should be sym-  
 318 metrical around  $\sigma_1$  (which is  $45^\circ$  clock-wise from the shear zone boundary for the dex-  
 319 tral shear sense modelled), which is generally observed in the models (with minor de-  
 320 viation due to stress rotation). In contrast to a homogeneous incompressible material,  
 321 the shear failure accommodates pure shear of the clasts, which are extended in the di-  
 322 rection of  $\sigma_2$ , as evident in the final clast geometries. Localised pure shear of the clasts  
 323 occurs in the incompressible model because it is compensated by simple shear within the  
 324 viscous matrix.

325 The Coulomb failure criteria predicts that failure will predominately occur on planes  
 326 orientated at angles  $\pm \tan^{-1}(\mu)/2 = \pm 17.5^\circ$  to  $\sigma_1$ . Numerical models only reproduce  
 327 this Coulomb failure angle when a high resolution is used relative to initial stress per-  
 328 turbations and shear bands (Kaus, 2010), otherwise shear failure occurs on planes ori-  
 329 entated closer to  $\pm 45^\circ$  to  $\sigma_1$  (called the Roscoe angles). Yielding zones localise in our  
 330 models due to the pressure-dependence of the Coulomb criteria, however are still rela-  
 331 tively broad ( $< 10m$ ) as no strain softening was incorporated. Failure occurs along bands  
 332 orientated at a range of angles between the Coulomb and Roscoe angles. The deviation  
 333 from the Coulomb angles may be due to the mesh resolution being too coarse in places  
 334 to sufficiently resolve stresses inside the clasts, though this deviation should not signif-  
 335 icantly affect clast deformation or stress magnitude.

### 336 4.3 General Melange Rheology

337 Each model in model-set A (Table 1) was repeated with the imposed stress bound-  
 338 ary condition varying through  $\tau = 21, 35, 70$  and  $140$  MPa, in order to characterise the  
 339 effective melange rheology (Figs. 2b and 4). The models share some of the character-  
 340 istics of the Bingham rheology; at low applied stress the effective melange viscosity can  
 341 be much higher than  $\eta_m$  ( $< 15\times$  for these models, depending on  $\phi$ ) and at high applied  
 342 stress the behaviour is dominated by viscous matrix deformation (the slope  $d\tau/d\dot{\epsilon}$  is sim-  
 343 ilar to that of the Bingham plastic prediction in Fig. 2b). However, for  $\phi = 0.61$  and  
 344  $\tau = 70$  MPa the fracturing causes the bulk strain-rate to be about  $2\times$  higher than ex-



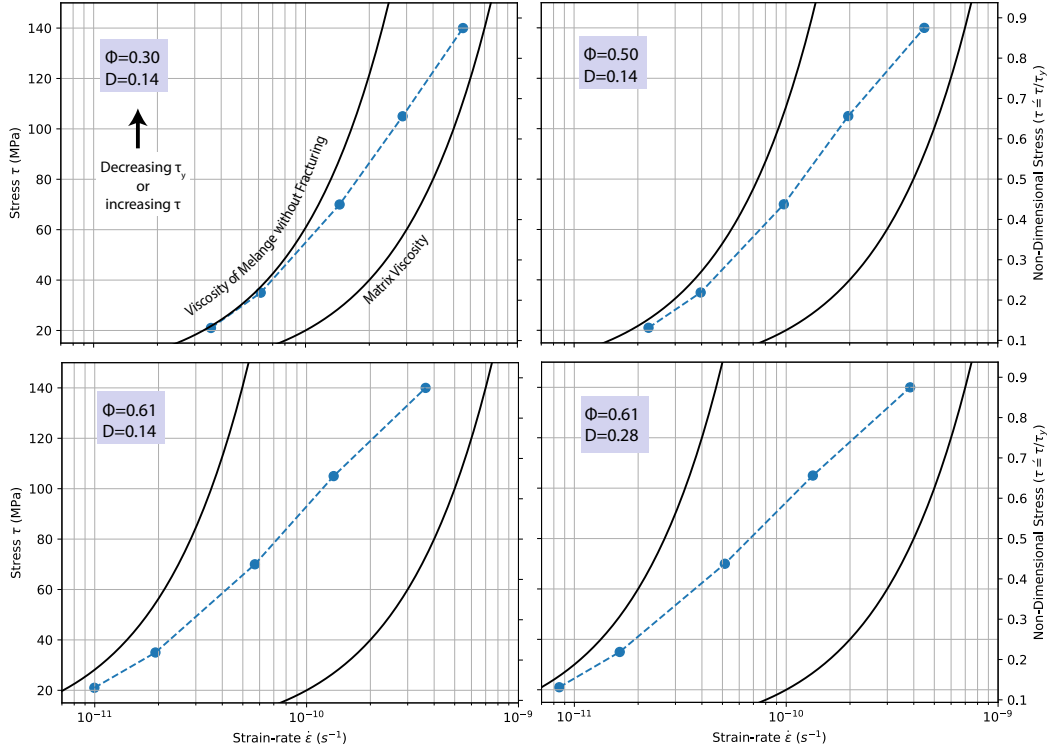


**Figure 4.** Rheologies of the models in model-set A, demonstrating that strain-rate increases exponentially with stress with a viscosity spanning that of *mélange* without fracturing at low  $\tau$ , to  $\eta_m$  at high  $\tau$ . The highest and lowest jamming occurs for  $\phi = 0.61$  and  $0.30$  respectively, which correspond to the highest and lowest strain-rate variation.

345 expected for the jammed *mélange*. This heralds a transition to predominately visco-brittle  
 346 deformation, which occurs at a lower stress than the 100 MPa predicted for the simpli-  
 347 fied Bingham rheology. This is due to the heterogeneous stress distribution in the clasts,  
 348 compared to the homogeneous stress assumed in the simplified model.

349 While the Bingham rheology is dominated by its viscous constituent when fractur-  
 350 ing occurs, the corresponding *mélange* rheology at high stress is non-Newtonian and strain-  
 351 rate increases exponentially with stress (i.e  $\tau$  appears to be logarithmically dependent  
 352 on  $\dot{\epsilon}$ ) for  $\tau \geq 35$  MPa ( $\tau' = 0.22$ ). Accordingly, fitting a power-law relationship of  $\dot{\epsilon} \propto$   
 353  $\sigma^n$  (though an exponential form provides a superior fit) gives  $n \sim 2$ , rather than the  
 354  $n > 10$  that would correspond to a highly non-linear rheology appropriate for a Reuss  
 355 mixture.

356 Mélange viscosity should always be greater or equal to the matrix viscosity when  
 357  $\tau \leq \tau_y$  and less or equal to an identical mélange in which fracturing is prohibited (i.e.  
 358 a model without frictional failure incorporated). These limits represent the strength end-  
 359 members (solid black curves, Fig. 4). All of the model bulk rheologies, regardless of  $\phi$ ,  
 360 follow a similar transition from one approximating the strong end-member (no fractur-  
 361 ing) at the lowest  $\tau$  (21 MPa or  $\tau' = 0.13$ ), to resembling the weak end-member (matrix-  
 362 dominated) for  $\tau' \approx 0.75 - 0.9$  (the higher end of the range for greater  $\phi$ ). This rheo-  
 363 logical trend demonstrates that all mélange models, regardless of jamming, are weakened  
 364 by fracturing even when  $\tau < \tau_y$ . While the bulk behaviour is bounded by the fracturing-  
 365 free and clast-free viscosity end-members, fracturing of a jammed mélange results in higher  
 366 strain-rate variation compared to these limiting cases (Fig. 4).

367 The exponential rheology  $\tau \propto \ln(\dot{\epsilon})$  arises because stress is not homogeneously  
 368 distributed across force chains. The probability distribution of clast points with a par-  
 369 ticular maximum shear stress are shown in Fig. 5 for models with a range of  $\tau$ . For  $\tau =$   
 370 21 and 35 MPa, the most common stress corresponds to the bulk shear stress  $\tau$ . More  
 371 clast particles have a stress higher than  $\tau$ , than those with a stress lower than  $\tau$ , result-  
 372 ing in a skewed normal distribution. Stresses higher than  $\tau$  result from stress ampli-  
 373 fication within force chains, which occurs to a varying degree. The normal distribution  
 374 shows, for example, that a stress amplification of  $2\times$  is more common than  $5\times$ . Only a  
 375 small number of force chains therefore fail when  $\tau \ll \tau_y$ . For an incremental increase  
 376 in scaled stress  $\tau'$  (corresponding to a  $\tau$  increase or a  $\tau_y$  decrease), a much higher num-  
 377 ber of clasts will fracture due to the non-linear stress distribution, resulting in a non-  
 378 linear rheology. Stress cannot exceed the failure criterion (it has the appearance of do-  
 379 ing so only due to the pressure-dependence introduced by  $\mu$ ), so with increasing  $\tau$ , clast  
 380 stress becomes more uniform as it is redistributed, resulting in a peak at  $\tau_y$  in Fig. 5.  
 381 By  $\tau = 70MPa$  ( $\tau' = 0.44$ ), most clasts are likely to be undergoing frictional failure.

#### 382 4.4 Frictional Weakening and Scaling

383 Two extra sets of models with  $\phi = 0.61$  and a constant yield stress  $\tau_y$  were run  
 384 (B and C, Table 1), for  $\tau_y = 50$  MPa and  $\tau_y = 200MPa$ , to explore how the visco-  
 385 brittle mélange rheology depends on the magnitude of clast frictional strength. These  
 386 models are used to test the hypothesised scaling relationships Eqns. 3 and 4, which can  
 387 then be used to rescale the existing models for any  $\tau_y$  and  $\eta_m$ .

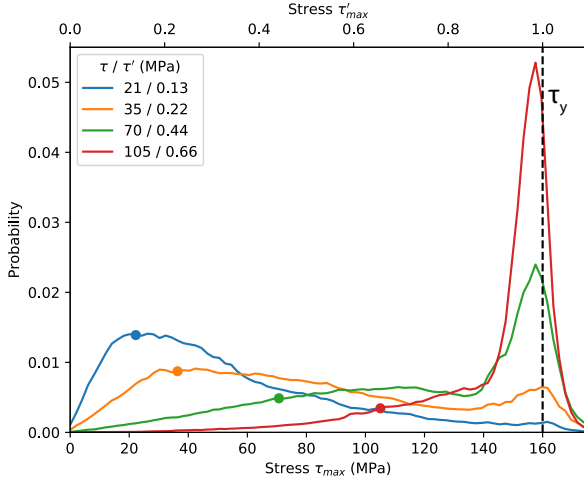
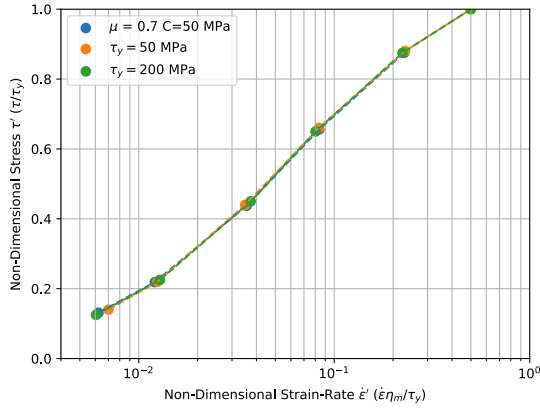


**Figure 5.** Maximum clast shear stress probability distribution, calculated from all Lagrangian particles identified as clast material, for  $\phi = 0.61$ ,  $D_{max} = 14\text{m}$ ,  $\tau_y \approx 160\text{MPa}$  (model-set A) and  $\tau$  ranging from 21 to 105 MPa (bulk stresses shown by points). At low  $\tau$ , stress follows a skew normal distribution, capturing heterogeneous stress amplification in force chains. At high  $\tau$ , stress is limited by  $\tau_y$ .

388 When non-dimensionalised, all model-sets with  $\phi = 0.61$  collapse onto the same  
 389 curve as predicted by scaling relations (Fig. 6a). The non-dimensionalised datasets with  
 390  $\mu = 0$  and  $\mu = 0.7$  (pressure independent and dependent  $\tau_y$  respectively) are identi-  
 391 cal, indicating that the pressure-dependence of the frictional law and therefore the op-  
 392 timal angle of frictional failure, does not influence the modelled bulk m $\acute{e}$ lange viscosity.

393 Fig. 6b demonstrates how strain-rate, and therefore velocity at the shear zone wall,  
 394 would increase if  $\tau_y$  were decreased for all of the clasts from 200 MPa to 50 MPa. The  
 395 scaling relationships are also used to calculate an intermediary case of  $\tau_y = 80$  MPa.  
 396 For  $\eta_m = 5 \times 10^{17}\text{Pa s}$  (assumed for Fig. 6b) and  $L = 100\text{m}$ , the average shear zone  
 397 boundary velocity  $V_{av}$  is about 2 cm/yr when  $\tau = 50$  MPa and  $\tau_y = 200$  MPa. This  
 398 is equivalent to  $\tau' = 0.25$ , which is sufficient for fracturing of clasts in the force chains  
 399 with the highest stress amplification (similar to Fig. 3b). In order to increase the veloc-  
 400 ity to 4 cm/yr, the clast yield strength needs to be reduced to  $\tau_y = 80$  MPa, for ex-  
 401 ample due to extreme strain-weakening as clasts fracture and distribute stress more evenly  
 402 across the force chains. Should  $\tau_y$  decrease to  $\tau_y = 50$  MPa, the velocity would increase  
 403 up to 16 cm/yr and the matrix would have a similar stress state to the clasts. This ex-

A)



B)

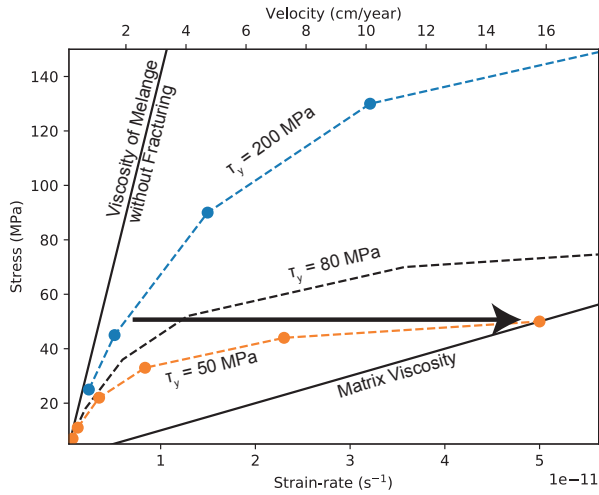


**Figure 6.** A) Model-sets A-C for  $\phi = 0.62$  and  $D_{max} = 14$  m, plotted for non-dimensional variables  $\tau'$  and  $\epsilon'$  (Eqs. 3 and 4). All data collapses onto one curve, confirming the scaling of stress using  $\tau_y$ . B) Model sets B and C, with a third case for  $\tau_y = 80$  MPa plotting using the scaling relationship and assuming  $\eta_m = 5 \times 10^{17}$  Pa s. Velocity is calculated assuming  $L = 100$  m. In the case of a constant  $\tau = 50$  MPa, deformation of *mélange* containing clasts with a high frictional strength,  $\tau_y = 200$  MPa, results in a velocity of  $2 \text{ cm yr}^{-1}$ . Reducing the clast frictional strength to 50 - 80 MPa (indicated by arrow) would increase this to 4 - 16  $\text{cm yr}^{-1}$ .

ample demonstrates that  $\tau'$  must be initially relatively low in order to generate a large strain-rate transient.

## 5 Discussion

We previously predicted, and have tested here, that fracturing could occur at relatively low applied shear stress in a *mélange* due to stress amplification, and this stress amplification could lead to a transient period of high strain-rate until the *mélange* jams again (Beall et al., 2019, Fig. 1a-b). Fracturing of clasts involved in force chains does indeed occur at low bulk stress, lowering the stress within the most load-bearing force chains. The fracturing also allows surrounding matrix to creep by releasing the jammed portion of the *mélange*. We found that clast fracturing can occur when  $\tau \approx 35$  MPa and  $\lambda = 0.8$ , even at 40 km depth. More generally, fracturing of multiple force chain clasts (Figs. 3 and 5) occurs when  $\tau > 0.22\tau_y$ . Fracturing of clasts within a *mélange* therefore may be just as indicative of a large strength contrast between the matrix and clast minerals, as extreme pore pressure (e.g. Webber et al., 2018).

The models verify that deformation of jammed *mélange* switches from clast to matrix dominated with increasing bulk stress, as predicted by the Bingham model. In a mixture of strong frictional clasts and weak viscous matrix, mixed visco-brittle deformation may record periods of high stress and/or weakened clasts and therefore high strain-rates (creating slip transients, e.g. SSEs), the duration of which may be related to transient effective stress and healing of fractures. Fracturing at low  $\tau$  does not, however, result in the dramatic switch to viscous deformation predicted by the Bingham model. This is because clast stresses follow a skew normal distribution and weakening of a force chain with the highest stress amplification does not weaken the force chains with less stress amplification (Fig. 5). This effect does, however, result in a non-linear bulk rheology, as each increment of stress weakens a greater number of force chains at higher stress. The highest strain-rate variation therefore results from changes to the proportion of clasts undergoing frictional failure. As force chains in a jammed material are critically organised, weakening of one force chain will lead to stress redistribution and an entire shear zone can be unjammed if clast weakening is high.

Compared to the weak stress-dependence of frictional sliding, viscous systems are extremely damped (stress-dependent). For example, the viscous strain-rate in a Bing-

435 ham material increases from zero, when fracturing begins, to  $\dot{\epsilon} \propto (\tau - \phi\tau_y)/\eta$  (Eq. 1).  
 436 A large  $\dot{\epsilon}$  therefore requires a large stress increase, large yield stress decrease, or a small  
 437 viscosity. Ando et al. (2012) inferred that  $\tau_y$  dynamically decreases by a similar mag-  
 438 nitude to the SSE stress drop (typically only 10-100 kPa; Brodsky & Mori, 2007) and  
 439 as a result predicted an extremely low  $\eta_m \sim 10^{11}$  Pa s in order to reproduce SSE ve-  
 440 locities. Stress drop in this system, however, could instead be limited by the viscous strain  
 441 during the SSE and is not necessarily related to  $\tau_y$  (as would be the case in a Reuss mix-  
 442 ture). A large dynamic decrease in  $\tau_y$  could drive the viscous strain-rate increase. In our  
 443 models, the frictional clast strength would need to reduce by  $\sim 75\%$  to result in an  $8\times$   
 444 increase in strain-rate (Fig. 6). Should large local variations in  $\tau_y$  occur, then velocities  
 445 could transiently increase from 2 up to 16 cm yr<sup>-1</sup> (plate velocity rates and higher) across  
 446 a 100 m thick *mélange* shear zone with  $\eta_m = 5 \times 10^{17}$  Pa s for  $\tau = 50$ MPa (Fig. 6).  
 447 The predicted matrix viscosity is relatively low, but can be reconciled with pressure-solution  
 448 creep (Niemeijer, 2018) or phyllosilicate flow laws (Mares & Kronenberg, 1993; Hilairt  
 449 et al., 2007).

450        Though the degree of frictional weakening predicted is significantly higher than the  
 451  $\sim 1\%$  weakening typical of frictional sliding at  $\sim 10^{-4}$  m s<sup>-1</sup> (Marone et al., 1990), it  
 452 could be explained by opening of extension or extensional-shear fractures in clasts, as  
 453 an opened fracture becomes a free surface. Such through-going fractures with a tensile  
 454 component are commonly observed in *mélange* clasts (Fig. 7a), and can be confined to  
 455 the clasts and form at an angle of  $80^\circ$  to discrete shear surfaces parallel to the shear zone  
 456 S-fabric (Fagereng, 2011b, 2013). These fractures accommodate extension of the clasts  
 457 (pure shear), which is kinematically consistent with simple shear partitioned into and  
 458 accommodated by the matrix. The *mélange* models also deform by this combination of  
 459 clast pure shear and matrix simple shear. If tensile fracturing were incorporated and favourable  
 460 over shear failure, the modelled conjugate failure planes would likely be replaced with  
 461 single tensile fractures. Localised visco-brittle clast deformation grades into distributed  
 462 viscous matrix deformation in the models, due to the choice of rheologies. These rhe-  
 463 ologies reflect observed *mélange* deformation, where fractures within and at the edges  
 464 of clasts grade into distributed matrix deformation at both thin-section and outcrop scale  
 465 (Fagereng & Sibson, 2010; Hayman & Lavier, 2014).

466        Simple shear of *mélange* may occur by combined deformation of a network of visco-  
 467 brittle matrix shears and connecting tensile fractures as described in several field exam-

468 ples (Fig. 7b; Sibson, 1996; Meneghini & Moore, 2007; Fagereng et al., 2010; Ujiie et al.,  
 469 2018). Such shear-fracture meshes within a ductile matrix are analogous to our model,  
 470 which is rate-limited by viscous deformation when clast fracturing occurs. This model  
 471 of local fracturing limited by surrounding ductile creep applies when there is no inter-  
 472 connected network of frictional material in the direction of simple shear. In our mod-  
 473 els, this condition is guaranteed by the assumption of a viscous matrix, however, extrap-  
 474 olation to nature requires that any fractures within the matrix (not modelled here) do  
 475 not extend/connect to form a more extensive shear fracture network. If localized shears  
 476 do develop in the matrix, experiments indicate that these may favour development of  
 477 frictional instabilities, but slip speed is still modulated by their interaction with surround-  
 478 ing creeping matrix (Scuderi et al., 2017).

479 Stress drop is controlled by the bulk shear zone simple shear strain, which unloads  
 480 the elastic upper plate. The stress drop in the Bingham model is therefore limited by  
 481 the magnitude of finite viscous strain during a strain transient, which is limited by the  
 482 period over which  $\tau_y$  is weak (i.e. healing). Significant weakening of  $\tau_y$  does not then nec-  
 483 essarily correspond to a large stress drop. Force chain clasts may fracture and weaken,  
 484 elastically loading the viscous matrix (through elastic strain which was neglected in our  
 485 models), before regaining their strength at a similar time-scale to viscous creep.

486 Slow slip events are often modelled as frictional ruptures governed by the empiri-  
 487 cal rate-and-state laws (Rubin, 2008). In these models, seismic rupture is prevented by  
 488 the similar strengths of the velocity strengthening and weakening parts, a weak stress-  
 489 dependence (rate-and-state properties  $a - b \approx -10^{-2}$  to  $-10^{-3}$ ), and the effective  
 490 normal stress being extremely small (on the order of kPa). A  $\sim$ kPa normal stress also  
 491 implies megathrust shear stresses of similar order, which is difficult to reconcile with es-  
 492 timates of 10 MPa order from geodynamic models (Lamb, 2006) and from creep rheol-  
 493 ogy and piezometry near the brittle-ductile transition (Angiboust et al., 2015). In con-  
 494 trast, in the rheologies used here, provided that the matrix material in the mélange is  
 495 velocity-strengthening, the strain-rate will always be limited by the matrix viscosity. In  
 496 our model, the effective normal stress can be  $\sim$ 10 MPa provided it is low enough so that  
 497 clast fracturing can occur by local stress amplification (assuming high viscosity contrast  
 498 and  $\phi$ ). Recent rupture models incorporating a microphysical model with viscous creep  
 499 were able to generate a combination of aseismic and seismic slip events, with an effec-  
 500 tive normal stress  $< 50$ MPa (van den Ende et al., 2018). Incorporating viscous damp-

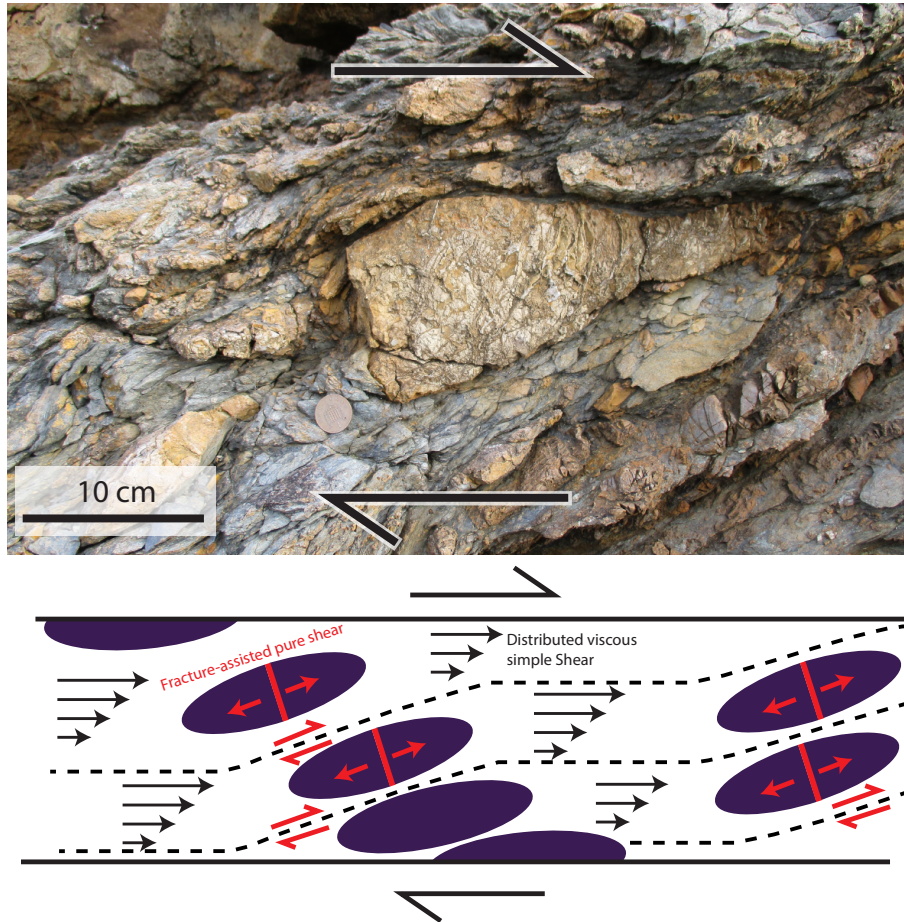


**Figure 7.** Top) Example of a fractured clast in the Gwna mélangé, Cemaes Bay, Anglesey, UK. This is the mélangé type locality region (Greenly, 1919) and is interpreted as a subduction accretionary complex (Kawai et al., 2007). Tensile fractures are confined to clasts and are kinematically consistent with distributed matrix shear strain. Bottom) Schematic of hypothesised strain-accumulation mechanisms. Mélangé simple shear is accommodated by pure shear of the clasts, which can occur through the opening of extension or extensional-shear fractures, and simple shear within the matrix.



501 ening into SSE models may therefore be a way to reconcile SSEs with regional stresses  
 502 of MPas, and help to explain their ubiquity in global subduction zones.

## 503 6 Conclusion

504 We have characterised the bulk rheology of a *mélange* consisting of strong visco-  
 505 brittle clasts embedded in a weak viscous matrix using numerical visco-plastic finite el-  
 506 ement models. When the clasts form a stress-bearing force-chain network, the bulk vis-  
 507 cosity of the *mélange* can be more than an order of magnitude stronger than the matrix  
 508 viscosity, in the absence of clast fracturing. When fracturing is allowed, clasts within the  
 509 most load-bearing force chains undergo frictional failure in models with bulk stress far  
 510 below the clast frictional strength,  $\tau \geq 0.22\tau_y$ , because of the stress amplification that  
 511 occurs within a shear zone with high viscosity contrasts. The fracturing of clasts acts  
 512 to homogenize stress in the force chain network and redistribute stress into viscous ma-  
 513 trix deformation. As deformation is limited by clast friction at low stress and rate-strengthening  
 514 viscous matrix creep at high stress, *mélange* rheology resembles a Bingham plastic. How-  
 515 ever, unlike a Bingham plastic, the switch from brittle to viscous deformation occurs across  
 516 a gradual transition, due to the heterogeneity of force chain stresses. This transition re-  
 517 sults in an effective rheology in the form of  $\dot{\epsilon} \propto \ln(\tau)$ , as the number of clasts fractur-  
 518 ing is more stress-sensitive at higher stress. This gradual transition also requires a large  
 519 stress increase or clast yield strength decrease ( $> 70\%$ ) in order to produce significant  
 520 bulk strain-rate increase ( $\sim 8\times$ ).

521 The models demonstrate how damped (i.e. significantly rate-strengthening) a visco-  
 522 brittle shear zone can be when no frictional slip surface spans it. Such a damped sys-  
 523 tem could still generate a period of high strain-rate with a negligible stress drop and at  
 524  $\sim 10$  MPa shear stress, if frictionally failing clasts temporarily lose most of their strength.  
 525 In this case, a matrix viscosity of  $< 5 \times 10^{17}$  Pa s could be reconciled with SSEs, com-  
 526 parable to rheological estimates. We suggest that this frictional weakening could occur  
 527 due to the opening of extension or extensional-shear fractures. This prediction needs to  
 528 be tested through future modelling incorporating tensile fracturing and elasticity. Sim-  
 529 ple shear across the modelled shear zone is accommodated by extension of clasts (pure  
 530 shear) and simple shear of the matrix. This model is supported by observed shear net-  
 531 works in exhumed *mélange*. The incorporation of viscous dampening into SSE rupture

532 models is likely to permit aseismic SSEs for a wider range of conditions than presently  
 533 thought, explaining their ubiquity in subduction zones globally.

### 534 **Acknowledgments**

535 This project has received funding from the European Research Council (ERC) un-  
 536 der the European Union's Horizon 2020 research and innovation program (starting grant  
 537 agreement 715836 MICA). The Hawk computing cluster (Cardiff University) was used  
 538 for all numerical calculations. We acknowledge the support of the Supercomputing Wales  
 539 project, which is part-funded by the European Regional Development Fund (ERDF) via  
 540 Welsh Government. Ellis was supported by MBIE Endeavour and core research funds  
 541 to GNS Science. The open-source geodynamic code Underworld is available at <http://www.underworldcode.org>,  
 542 and model parameters required to replicate the results are detailed in the manuscript.

### 543 **References**

- 544 Ando, R., Takeda, N., & Yamashita, T. (2012). Propagation dynamics of seismic  
 545 and aseismic slip governed by fault heterogeneity and Newtonian rheology.  
 546 *Journal of Geophysical Research B: Solid Earth*. doi: 10.1029/2012JB009532
- 547 Angiboust, S., Kirsch, J., Oncken, O., Glodny, J., Monié, P., & Rybacki, E. (2015).  
 548 Probing the transition between seismically coupled and decoupled segments  
 549 along an ancient subduction interface. *Geochemistry, Geophysics, Geosystems*.  
 550 doi: 10.1002/2015GC005776
- 551 Beall, A., Fagereng, Å., & Ellis, S. (2019). Strength of Strained Two-Phase Mix-  
 552 tures: Application to Rapid Creep and Stress Amplification in Subduction  
 553 Zone Mélange. *Geophysical Research Letters*. doi: 10.1029/2018GL081252
- 554 Behr, W. M., & Becker, T. W. (2018). Sediment control on subduction plate speeds.  
 555 *Earth and Planetary Science Letters*. doi: 10.1016/j.epsl.2018.08.057
- 556 Birren, T., & Reber, J. E. (2019). The impact of rheology on the transition from  
 557 stick-slip to creep in a semi-brittle analog. *Journal of Geophysical Research:*  
 558 *Solid Earth*. doi: 10.1029/2018jb016914
- 559 Bos, B., & Spiers, C. J. (2001). Experimental investigation into the microstruc-  
 560 tural and mechanical evolution of phyllosilicate-bearing fault rock under  
 561 conditions favouring pressure solution. *Journal of Structural Geology*. doi:  
 562 10.1016/S0191-8141(00)00184-X

- 563 Brodsky, E. E., & Mori, J. (2007). Creep events slip less than ordinary earthquakes.  
564 *Geophysical Research Letters*. doi: 10.1029/2007GL030917
- 565 Duarte, J. C., Schellart, W. P., & Cruden, A. R. (2015). How weak is the sub-  
566 duction zone interface? *Geophysical Research Letters*. doi: 10.1002/  
567 2014GL062876
- 568 Fagereng, Å. (2011a). Frequency-size distribution of competent lenses in a block-in-  
569 matrix mélange: Imposed length scales of brittle deformation? *Journal of Geo-*  
570 *physical Research: Solid Earth*. doi: 10.1029/2010JB007775
- 571 Fagereng, Å. (2011b). Geology of the seismogenic subduction thrust interface. *Geo-*  
572 *logical Society, London, Special Publications*. doi: 10.1144/sp359.4
- 573 Fagereng, Å. (2013). On stress and strain in a continuous-discontinuous shear zone  
574 undergoing simple shear and volume loss. *Journal of Structural Geology*. doi:  
575 10.1016/j.jsg.2012.02.016
- 576 Fagereng, Å., & den Hartog, S. A. M. (2016). Subduction megathrust creep gov-  
577 erned by pressure solution and frictional–viscous flow. *Nature Geoscience*. doi:  
578 10.1038/ngeo2857
- 579 Fagereng, Å., Hillary, G. W., & Diener, J. F. (2014). Brittle-viscous de-  
580 formation, slow slip, and tremor. *Geophysical Research Letters*. doi:  
581 10.1002/2014GL060433
- 582 Fagereng, Å., Remitti, F., & Sibson, R. H. (2010). Shear veins observed within  
583 anisotropic fabric at high angles to the maximum compressive stress. *Nature*  
584 *Geoscience*. doi: 10.1038/ngeo898
- 585 Fagereng, Å., & Sibson, R. H. (2010). Mélange rheology and seismic style. *Geology*.  
586 doi: 10.1130/G30868.1
- 587 Festa, A., Dilek, Y., Pini, G. A., Codegone, G., & Ogata, K. (2012). Mechanisms  
588 and processes of stratal disruption and mixing in the development of mélanges  
589 and broken formations: Redefining and classifying mélanges. *Tectonophysics*.  
590 doi: 10.1016/j.tecto.2012.05.021
- 591 Fisher, D., & Byrne, T. (1987). Structural evolution of underthrust sediments,  
592 Kodiak Islands, Alaska. *Tectonics*. doi: 10.1029/TC006i006p00775
- 593 Fullsack, P. (1995). An arbitrary Lagrangian-Eulerian formulation for creeping flows  
594 and its application in tectonic models. *Geophysical Journal International*. doi:  
595 10.1111/j.1365-246X.1995.tb05908.x

- 596 Goswami, A., & Barbot, S. (2018). Slow-slip events in semi-brittle serpentinite fault  
597 zones. *Scientific Reports*. doi: 10.1038/s41598-018-24637-z
- 598 Greenly, E. (1919). *The geology of Anglesey*. HM Stationery Office.
- 599 Grigull, S., Krohe, A., Moos, C., Wassmann, S., & Stöckhert, B. (2012). "Order  
600 from chaos": A field-based estimate on bulk rheology of tectonic mélanges  
601 formed in subduction zones. *Tectonophysics*. doi: 10.1016/j.tecto.2011.11.004
- 602 Handy, M. R. (1994). Flow laws for rocks containing two non-linear viscous phases:  
603 A phenomenological approach. *Journal of Structural Geology*. doi: 10.1016/  
604 0191-8141(94)90035-3
- 605 Hayman, N. W., Ducloué, L., Foco, K. L., & Daniels, K. E. (2011). Granu-  
606 lar Controls on Periodicity of Stick-Slip Events: Kinematics and Force-  
607 Chains in an Experimental Fault. *Pure and Applied Geophysics*. doi:  
608 10.1007/s00024-011-0269-3
- 609 Hayman, N. W., & Lavier, L. L. (2014, mar). The geologic record of deep episodic  
610 tremor and slip. *Geology*, 42(3), 195–198. doi: 10.1130/G34990.1
- 611 Hilaret, N., Reynard, B., Wang, Y., Daniel, I., Merkel, S., Nishiyama, N., & Petit-  
612 girard, S. (2007). High-pressure creep of serpentine, interseismic deformation,  
613 and initiation of subduction. *Science*. doi: 10.1126/science.1148494
- 614 Hyndman, R. D., Yamano, M., & Oleskevich, D. A. (1997). The seismogenic zone of  
615 subduction thrust faults. *Island Arc*. doi: 10.1111/j.1440-1738.1997.tb00175.x
- 616 Jaeger, J. C. J. C., Cook, N. G. W., & Zimmerman, R. W. (2007). *Fundamentals of*  
617 *rock mechanics*. Blackwell Pub.
- 618 Kaproth, B. M., & Marone, C. (2013). Slow earthquakes, preseismic veloc-  
619 ity changes, and the origin of slow frictional stick-slip. *Science*. doi:  
620 10.1126/science.1239577
- 621 Karato, S.-i. (2012). *Deformation of Earth Materials*. doi: 10.1017/  
622 cbo9780511804892
- 623 Kaus, B. J. (2010). Factors that control the angle of shear bands in geodynamic nu-  
624 merical models of brittle deformation. *Tectonophysics*. doi: 10.1016/j.tecto  
625 .2009.08.042
- 626 Kawai, T., Windley, B. F., Terabayashi, M., Yamamoto, H., Maruyama, S., Omori,  
627 S., ... Isozaki, Y. (2007). Geotectonic framework of the Blueschist Unit on  
628 Anglesey-Lleyn, UK, and its role in the development of a Neoproterozoic accre-

- 629           tionary orogen. *Precambrian Research*. doi: 10.1016/j.precamres.2006.11.002
- 630 Kitamura, Y., Sato, K., Ikesawa, E., Ikehara-Ohmori, K., Kimura, G., Kondo, H.,  
631           ... Masago, H. (2005). Mélange and its seismogenic roof décollement: A plate  
632           boundary fault rock in the subduction zone - An example from the Shimanto  
633           Belt, Japan. *Tectonics*. doi: 10.1029/2004TC001635
- 634 Lamb, S. (2006). Shear stresses on megathrusts: Implications for mountain build-  
635           ing behind subduction zones. *Journal of Geophysical Research*. doi: 10.1029/  
636           2005JB003916
- 637 Lavier, L. L., Bennett, R. A., & Duddu, R. (2013). Creep events at the brittle duc-  
638           tile transition. *Geochemistry, Geophysics, Geosystems*. doi: 10.1002/ggge  
639           .20178
- 640 Leeman, J. R., Marone, C., & Saffer, D. M. (2018). Frictional Mechanics of Slow  
641           Earthquakes. *Journal of Geophysical Research: Solid Earth*. doi: 10.1029/  
642           2018JB015768
- 643 Liu, Y., & Rice, J. R. (2005). Aseismic slip transients emerge spontaneously in  
644           three-dimensional rate and state modeling of subduction earthquake sequences.  
645           *Journal of Geophysical Research: Solid Earth*. doi: 10.1029/2004JB003424
- 646 Luo, Y., & Ampuero, J. P. (2018). Stability of faults with heterogeneous friction  
647           properties and effective normal stress. *Tectonophysics*. doi: 10.1016/j.tecto  
648           .2017.11.006
- 649 Mares, V. M., & Kronenberg, A. K. (1993). Experimental deformation of muscovite.  
650           *Journal of Structural Geology*. doi: 10.1016/0191-8141(93)90156-5
- 651 Marone, C., Raleigh, C. B., & Scholz, C. H. (1990). Frictional behavior and consti-  
652           tutive modeling of simulated fault gouge. *Journal of Geophysical Research*. doi:  
653           10.1029/JB095iB05p07007
- 654 Meneghini, F., & Moore, J. C. (2007). Deformation and hydrofracture in a sub-  
655           duction thrust at seismogenic depths: The Rodeo Cove thrust zone, Marin  
656           Headlands, California. *Bulletin of the Geological Society of America*. doi:  
657           10.1130/B25807.1
- 658 Moresi, L., & Solomatov, V. (1998). Mantle convection with a brittle lithosphere:  
659           thoughts on the global tectonic styles of the Earth and Venus. *Geophysical*  
660           *Journal International*. doi: 10.1046/j.1365-246X.1998.00521.x
- 661 Niemeijer, A. R. (2018, dec). Velocity-dependent slip weakening by the combined op-

- 662           eration of pressure solution and foliation development. *Scientific Reports*, 8(1),  
663           4724. doi: 10.1038/s41598-018-22889-3
- 664   Obara, K., Hirose, H., Yamamizu, F., & Kasahara, K.   (2004).   Episodic slow slip  
665           events accompanied by non-volcanic tremors in southwest Japan subduction  
666           zone. *Geophysical Research Letters*. doi: 10.1029/2004GL020848
- 667   Raimbourg, H., Tadahiro, S., Asuka, Y., Haruka, Y., & Kimura, G.   (2009).   Hori-  
668           zontal shortening versus vertical loading in accretionary prisms. *Geochemistry,*  
669           *Geophysics, Geosystems*. doi: 10.1029/2008GC002279
- 670   Reber, J. E., Lavier, L. L., & Hayman, N. W.   (2015).   Experimental demonstration  
671           of a semi-brittle origin for crustal strain transients. *Nature Geoscience*. doi: 10  
672           .1038/ngeo2496
- 673   Rogers, G., & Dragert, H.   (2003).   Episodic tremor and slip on the Cascadia subduc-  
674           tion zone: The chatter of silent slip. *Science*. doi: 10.1126/science.1084783
- 675   Rowe, C. D., Meneghini, F., & Moore, J. C.   (2011).   Textural record of the seismic  
676           cycle: strain-rate variation in an ancient subduction thrust. *Geological Society,*  
677           *London, Special Publications*. doi: 10.1144/SP359.5
- 678   Rowe, C. D., Moore, J. C., & Remitti, F.   (2013).   The thickness of subduction plate  
679           boundary faults from the seafloor into the seismogenic zone. *Geology*. doi: 10  
680           .1130/G34556.1
- 681   Rubin, A. M.   (2008).   Episodic slow slip events and rate-and-state friction. *Journal*  
682           *of Geophysical Research: Solid Earth*. doi: 10.1029/2008JB005642
- 683   Saffer, D. M., & Tobin, H. J.   (2011).   Hydrogeology and Mechanics of Subduction  
684           Zone Forearcs: Fluid Flow and Pore Pressure.   *Annual Review of Earth and*  
685           *Planetary Sciences*. doi: 10.1146/annurev-earth-040610-133408
- 686   Scholz, C. H.   (1998).   *Earthquakes and friction laws*. doi: 10.1038/34097
- 687   Schwartz, S. Y., & Rokosky, J. M.   (2007).   *Slow slip events and seismic tremor at*  
688           *circum-pacific subduction zones*. doi: 10.1029/2006RG000208
- 689   Scuderi, M. M., Collettini, C., Viti, C., Tinti, E., & Marone, C.   (2017).   Evolution  
690           of shear fabric in granular fault gouge from stable sliding to stick slip and  
691           implications for fault slip mode. *Geology*. doi: 10.1130/G39033.1
- 692   Sibson, R. H.   (1996).   Structural permeability of fluid-driven fault-fracture meshes.  
693           *Journal of Structural Geology*. doi: 10.1016/0191-8141(96)00032-6
- 694   Skarbek, R. M., Rempel, A. W., & Schmidt, D. A.   (2012).   Geologic heterogeneity

- 695 can produce aseismic slip transients. *Geophysical Research Letters*. doi: 10  
 696 .1029/2012GL053762
- 697 Ujiie, K., Saishu, H., Fagereng, Å., Nishiyama, N., Otsubo, M., Masuyama, H., &  
 698 Kagi, H. (2018). An Explanation of Episodic Tremor and Slow Slip Con-  
 699 strained by Crack-Seal Veins and Viscous Shear in Subduction Mélange. *Geo-*  
 700 *physical Research Letters*. doi: 10.1029/2018GL078374
- 701 van den Ende, M. P., Chen, J., Ampuero, J. P., & Niemeijer, A. R. (2018).  
 702 A comparison between rate-and-state friction and microphysical mod-  
 703 els, based on numerical simulations of fault slip. *Tectonophysics*. doi:  
 704 10.1016/j.tecto.2017.11.040
- 705 Wallace, L. M., & Beavan, J. (2010). Diverse slow slip behavior at the Hikurangi  
 706 subduction margin, New Zealand. *Journal of Geophysical Research: Solid*  
 707 *Earth*. doi: 10.1029/2010JB007717
- 708 Wassmann, S., & Stöckhert, B. (2013). *Rheology of the plate interface - Disso-*  
 709 *lution precipitation creep in high pressure metamorphic rocks*. doi: 10.1016/j  
 710 .tecto.2013.09.030
- 711 Webber, S., Ellis, S., & Fagereng, Å. (2018). “Virtual shear box” experiments of  
 712 stress and slip cycling within a subduction interface mélange. *Earth and Plane-*  
 713 *tary Science Letters*. doi: 10.1016/j.epsl.2018.01.035